IIETA International Information and Engineering Technology Association
Advancing the World of Information and Engineering

Mathematical Modelling of Engineering Problems
Vol. 13, No. 1, February, 2026, pp. 87-98
Journal homepage: http://iieta.org/journals/mmep

Electrochemical Desalination via Capacitive Deionization: COMSOL Simulation with Ag/rGO Conductive Concrete Electrodes

Zahraa Naji Kareem*, Ahmed Ali Moosa, Ammar A. H. Al-Filfily

Department of Materials Engineering Technology, Engineering Technical College, Middle Technical University, Baghdad 10074, Iraq

Corresponding Author Email: aac0026@mtu.edu.iq

https://doi.org/10.18280/mmep.130109

Received: 3 November 2025
Revised: 13 January 2026
Accepted: 25 January 2026
Available online: 28 February 2026

Keywords:
COMSOL Multiphysics simulation, capacitive deionization, electrochemical desalination, conductive concrete electrodes

ABSTRACT

This study integrates numerical simulation and performance evaluation of a capacitive deionization (CDI) system employing conductive concrete electrodes doped with Ag/rGO nanocomposites for desalinating brackish and high-salinity water. Using COMSOL Multiphysics 6.3, a two-dimensional, membrane-free CDI cell was modeled to simulate ion transport, electroadsorption, and electric field distribution across stagnant NaCl solutions. Parametric analyses were conducted to investigate the impact of applied voltage (5–25 V), electrode spacing (5–12.5 cm), and initial salinity (250–8000 ppm) on the desalination efficiency of the CDI system. Additionally, large-scale simulations were performed for 1 m³ and 10 m³ tanks to estimate potential production rates. The results indicate that increasing the applied voltage from 5 V to 25 V reduced the NaCl concentration by up to 78%, with charge efficiencies ranging from 0.72 to 0.89. Reducing the electrode spacing to 5 cm improved ion removal by approximately 45% compared with a 12.5 cm gap. At larger scales, the simulations predicted daily freshwater outputs of about 2,000 L for 1 m³ tanks operated at 35–45 V, and up to 15,000 L for 10 m³ tanks at 60–80 V. Collectively, these findings demonstrate that Ag/rGO-modified conductive concrete is an effective CDI electrode material, capable of delivering scalable and energy-efficient desalination for high-salinity waters such as those found in Basra, Iraq.

1. INTRODUCTION

Electrochemical water desalination is an emerging technology that removes salt ions from saline water by applying an electrical potential as the driving force [1]. Among the different electrochemical approaches, electrodialysis (ED) and capacitive deionization (CDI) have attracted particular interest because of their ion selectivity, relatively low energy demand, and promising economic feasibility for brackish water treatment and reuse applications. CDI, in particular, offers a straightforward cell configuration and a favorable environmental profile, which make it an appealing option for decentralized desalination. Nevertheless, conventional CDI units are limited by side reactions that occur at elevated voltages and by incomplete salt removal, challenges that continue to drive efforts toward improved electrode materials, modified architectures, and hybrid CDI designs [2, 3].

To overcome these challenges, researchers have explored the use of nanostructured electrode materials, with silver-reduced graphene oxide (Ag/rGO) nanocomposites receiving particular attention. The incorporation of nanomaterials enhances CDI electrode performance by providing a large surface area, high electrical conductivity, chemical and structural stability, well-tailored porosity, and reliable cycling durability [4]. CDI operates by adsorbing ions on charged electrode surfaces during voltage application, and has also proven effective in removing heavy metals and organic contaminants. Compared to membrane-based techniques, CDI offers reduced membrane fouling, lower maintenance, and potentially superior energy performance [5, 6]. In a typical CDI cycle, ions are adsorbed onto electrodes during charging and are released during discharge via polarity reversal [7].

The foundational concepts of CDI were established in seminal works by Farmer et al. [8], who first demonstrated the principle of ion electrosorption on porous carbon electrodes, and by Biesheuvel [9] and Biesheuvel and Bazant [10], who developed quantitative models capturing the coupled transport, adsorption, and electrostatic phenomena in CDI cells. These studies laid the groundwork for subsequent modeling approaches, emphasizing the importance of electric double-layer (EDL) formation, ion diffusion, and electrode geometry in determining desalination performance.

Several recent studies highlight the predictive value of numerical simulation in CDI design. Jiang et al. [11] conducted 2D simulations incorporating EDL effects, showing that voltage and geometry significantly affect electro-sorption. Studies [12, 13] validated COMSOL models for porous carbon electrodes in stagnant saline media, while Seyedhassantehrani and Palko [14] demonstrated the optimization potential of such models. Haverkort et al. [15] further explored transient outlet

concentration dynamics, emphasizing the role of electric field gradients. These studies collectively underscore the importance of simulation in guiding practical CDI optimization.

Several studies have investigated the application of carbon-based electrodes for CDI, demonstrating effective ion adsorption and regeneration capabilities [16, 17]. Recent work by Rommerskirchen et al. [18] explored the scalability of CDI systems with novel electrode materials. However, limited attention has been given to conductive concrete, despite its advantages in structural robustness, cost-effectiveness, and multifunctionality. Previous applications of conductive concrete have focused mainly on deicing, self-sensing, and electromagnetic shielding, with little emphasis on water desalination. Therefore, this study addresses the gap by integrating Ag/rGO nanocomposites into conductive concrete electrodes and evaluating their performance in electrochemical desalination systems.

Building on this foundation, the present work developed a computational framework for modeling CDI with conductive concrete electrodes. The model was implemented in COMSOL Multiphysics 6.3 and combined the Electric Currents, Transport of Diluted Species, and Secondary Current Distribution interfaces to represent the coupled electrochemical processes. Particular emphasis was placed on maintaining numerical stability by simplifying the governing equations where possible, reducing nonlinearities to enable direct time-dependent simulations, and designing the framework to remain modular so it can be adapted to a variety of electrode geometries and material properties.

Conductive concrete is generally less conductive than pure carbon electrodes. Researchers have improved its properties by incorporating conductive fillers such as carbon fibers, graphite, graphene, or metallic particles. Over the past two decades, this modified form of concrete has been applied in diverse fields—for example, as a deicing material [19, 20], in structural health monitoring through self-sensing [21, 22], and in functional roles such as electromagnetic shielding [23] and cathodic protection [24]. In the present work, silver-reduced graphene oxide (Ag/rGO) nanocomposites were added to the concrete matrix to lower resistive losses. The intent was to establish continuous conductive pathways that could make the material more suitable for electrochemical desalination applications.

This study aims to develop a reliable and computationally efficient numerical model for CDI systems incorporating Ag/rGO-based conductive concrete electrodes. In contrast to earlier research that mainly considered carbon-based electrodes, the present work examines conductive concrete as a viable alternative. It evaluates its desalination performance across varying voltages, salinity levels, and electrode spacings.

2. METHODOLOGY

To complement the experimental investigation of electrochemical water desalination using conductive concrete electrodes, a comprehensive numerical model was developed using COMSOL Multiphysics 6.3. This simulation replicates the ion removal mechanisms in a membrane-free CDI system by modeling the electroadsorption of sodium (Na^+) and chloride (Cl^-) ions onto oppositely charged porous electrodes under direct current (DC) voltage.

The model integrates Electrostatics, Transport of Diluted Species, and Secondary Current Distribution physics to capture the electrochemical interactions within a stagnant water domain. A two-dimensional domain was selected, leveraging the CDI cell's horizontal symmetry and the unidirectional electric field across the electrode gap [13].

2.1 Model geometry and physics interfaces

The simulation adopts a two-dimensional cross-section of the experimental CDI configuration, consisting of two square porous electrodes (50 mm × 50 mm) separated by a stagnant saline gap of 10 cm. The complete unit spans 30 cm (length) × 20 cm (width) × 5 cm (height). Figure 1 illustrates Na^+ migration toward the cathode and Cl^- toward the anode under the influence of the applied voltage.

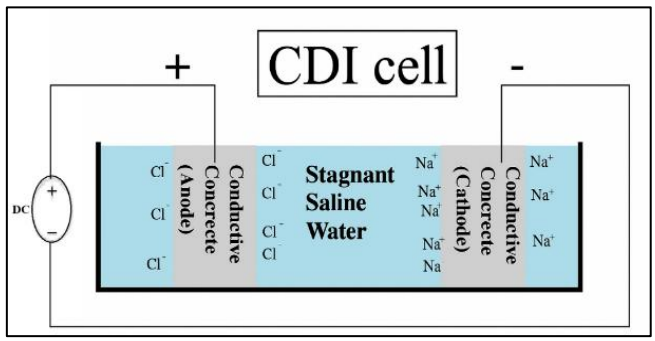

Figure 1. Schematic representation of the membrane-free capacitive deionization (CDI) cell with conductive concrete electrodes and stagnant saline water

The following physics were coupled:

• Secondary Current Distribution for simulating electronic and ionic conduction.

• Transport of Diluted Species for modeling Na^+ and Cl^- transport.

Modified Donnan Adsorption module for ion storage in micropores, based on the thermodynamically consistent framework of Nordstrand et al. [13].

Material properties were defined as follows:

• Electrodes: Porous conductive concrete doped with Ag/rGO, electrical conductivity = 0.1 S/m.

• Electrolyte: Stationary NaCl solution (5–20 mM), with ion diffusivities of 1.33×10^{-9} m²/s (Na^+) and 2.03×10^{-9} m²/s (Cl^-).

• Temperature: Baseline of 20°C, with additional simulations at elevated temperatures.

• Voltage: DC voltages ranging from 5 to 25 V applied across electrode boundaries.

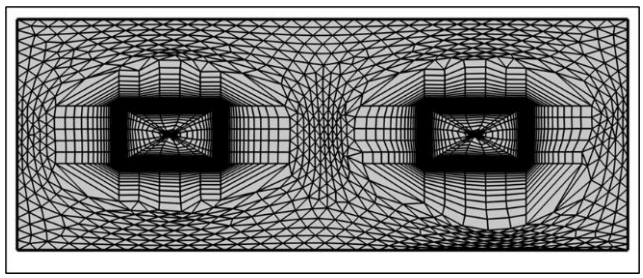

Figure 2. Finite element mesh structure used in COMSOL, showing boundary-layer refinement near electrodes and coarser meshing in the bulk saline region

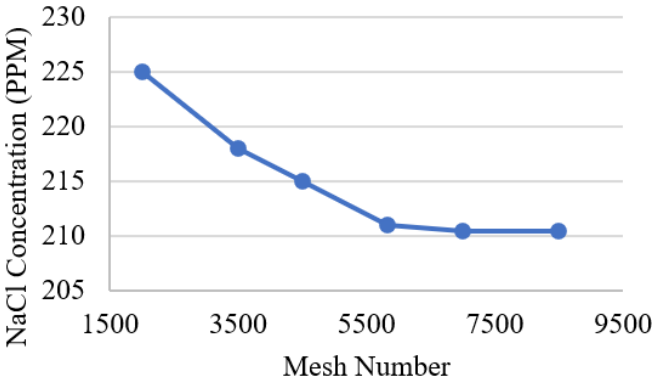

Figure 3. Variation of the NaCl concentration parts per million (ppm) with the mesh numbers at 5 voltages applied, 10 cm gap between electrodes, and 20°C

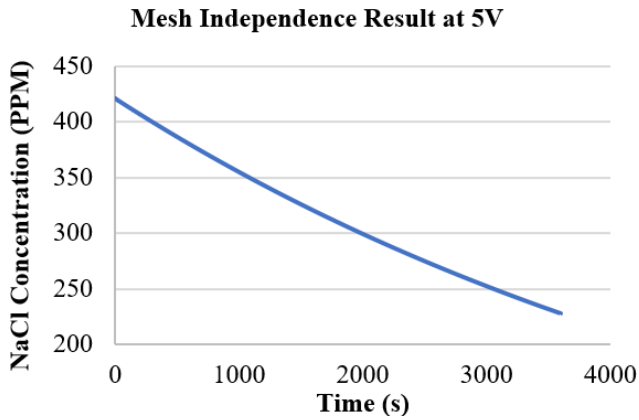

Figure 4. Mesh-independence verification showing stable NaCl reduction over time

2.2 Finite element mesh

To resolve gradients in EDL regions, a 50-layer boundary mesh was applied to each electrode interface (thickness: 5 mm, stretch factor: 1.2). The bulk saline domain was meshed with coarser triangular elements to optimize simulation speed.

A mesh convergence study verified independence from element count. As shown in Figure 2, the final outlet NaCl concentration stabilized (< 211 parts per million (ppm)) once the domain mesh exceeded 5826 elements, validating mesh adequacy.

To verify mesh adequacy, a grid-convergence study was performed by comparing the final outlet NaCl concentration at progressively finer mesh densities. Figure 3 shows the relationship between the total element count and the final concentration obtained at 5 V applied voltage, a 10 cm electrode gap, and 20°C ambient temperatures. The solution stabilises below 211 ppm when the mesh exceeds 5826 domain elements (with a 50-layer boundary refinement), indicating mesh independence. Consequently, this mesh configuration was adopted for all subsequent simulations. Figure 4 confirms that with the refined mesh, concentration decay remained stable and free of oscillations, ensuring reliable simulation of electroadsorption dynamics.

2.3 Modelling assumptions

The following assumptions were adopted to simplify the numerical model while capturing the essential physics of CDI using conductive concrete electrodes:

- Binary, dilute NaCl electrolyte; effective diffusivity *De* for both ions [15].
- Quasi-electroneutrality is enforced in macropores (i.e., no space charge), while space-charge effects are resolved inside micropores via the modified Donnan (mD) model.
- Water is treated as incompressible and stationary ($u = 0$), reflecting a no-flow (batch-mode) CDI operation.
- A constant volumetric capacitance C_m and constant attraction potential μ_{att} are assumed throughout the micropore domain.
- No ion-exchange membrane is included between the electrodes, similar to the experimental cell design.
- Porous conductive concrete electrodes are modeled as microporous media that adsorb ions following the Donnan equilibrium governed by μ_{att}.

2.4 Governing equations

2.4.1 Electronic and ionic conduction

- **In the electrolyte:**

$$\nabla . \left(\sigma_l \nabla \varnothing_l\right) = 0, \sigma_l = \frac{F^2}{RT} \sum_i z_i^2 D_i c_i \quad (1)$$

where, σ_l is updated with the instantaneous ion concentration [3]. ϕ_l is the electrolyte potential; σ_l is the ionic conductivity, dynamically updated based on local concentration; D_i is the diffusion coefficient (m²/s for ion (Na, Cl); z_i is the charge number of species i; c_i is the concentration of species i; F is the faraday constant; R is the universal gas constant; T is the temperature.

- **In the concrete matrix (electrode):**

$$\nabla . \left(\sigma_s \nabla \varnothing_s\right) = 0 \quad (2)$$

where, ϕ_s is the solid-phase potential and σ_s is the electronic conductivity of the concrete matrix.

2.4.2 Ion Transport—Transport of Diluted Species (interface)

For each species i (Na^+, Cl^-)

$$\frac{\partial(\varepsilon_p c_i)}{\partial t} + \nabla . \left(- D_{eff,i} \nabla c_i\right) = R_i \quad (3)$$

where, c_i is the ion concentration (mol/m³); ε_p is the porosity with $D_{eff,i} = \varepsilon_p^{3/2} D_i$ (Bruggeman correction); R_i is the reaction/source term from adsorption.

- **Alternative Nernst-Planck:**

$$\frac{\partial c_i}{\partial t} + \nabla . N_i = R_i \quad (4)$$

$$N_i = - D_i \nabla c_i - z_i u_i F c_i \nabla F \quad (5)$$

where, u_i is the ion mobility; V is electric potential.

2.4.3 Modified-Donnan adsorption

Adsorption within micropores is modeled by the modified Donnan approach.

- **Micropore concentration:**

$$c_{m,i=c_{M,i}} e^{-z\Delta\emptyset D + \mu_{att}} \quad (6)$$

- **Micropore charge:**

$$q_m = -2\ c\ e^{\mu_{att}} sinh\ [\Delta\emptyset^- D] \tag{7}$$

where, $\Delta\emptyset^- D = \Delta\emptyset D/V_T$ and $V_T = RT/F$ [15]; $\Delta\phi D$ is the Donnan potential drop; VT=FRT refers to the thermal voltage; μ_{att} is the non-electrostatic attractive potential.

- **Micropore potential-charge relation:**

$$\Delta\emptyset_m = -\frac{2F}{C_m} q_m \tag{8}$$

where, C_m is the capacitance of the micropore layer; q_m is the stored charge.

2.4.4 Charge balance and Randles analogy

The local current density is modeled using a capacitive Randles circuit analogy:

$$i_{tot} = C_{dl} \frac{\partial}{\partial t} \left(\varnothing_s - \varnothing_t\right) + \frac{\varnothing_s - \varnothing_t}{R_L} \tag{9}$$

Eq. (9) satisfies the classic Randles circuit used for zero-dimensional validation. C_{dl} is the double-layer capacitance (F/m²); R_L is the leakage resistance; ϕ_s and ϕ_t present the solid and electrolyte potentials, respectively.

This equation is used to validate the time-domain charging behavior against a zero-dimensional capacitor model.

2.4.5 Stern layer capacitance model

The volumetric capacitance within micropores is defined as:

$$C = C_{ref} + \alpha \left(z_{Na^+ cNa^+, micro} + z_{Cl^- cCl^-, micro}\right)^2 \tag{10}$$

where, C is the total volumetric capacitance (F/m³); C_{ref} is the reference (intrinsic) capacitance; α is the capacitance sensitivity coefficient; and *micro* is the micropore ion concentrations.

2.4.6 Micropore attractive potential

To account for non-electrostatic interactions:

$$\mu_{att} = \frac{E}{\left(c_{sum} + 10^{-9}\right) K_b T N_A} \tag{11}$$

where, E is the attractive energy constant; c_{sum} is the total micropore ion concentration; K_b is the Boltzmann constant; T is the temperature, and N_A is Avogadro's number.

2.4.7 Empirical charge efficiency relation

The charge efficiency Λ varies with voltage:

$$\Lambda = 1 - \frac{V_0}{V_{ext}} \tag{12}$$

Eq. (12) is adapted from the dynamic Langmuir isotherm to approximate voltage-dependent ion adsorption behaviour.

2.5 Number of iterations and convergence criterion

A time-dependent solver using the Backward Differentiation Equation (BDF) was configured with:

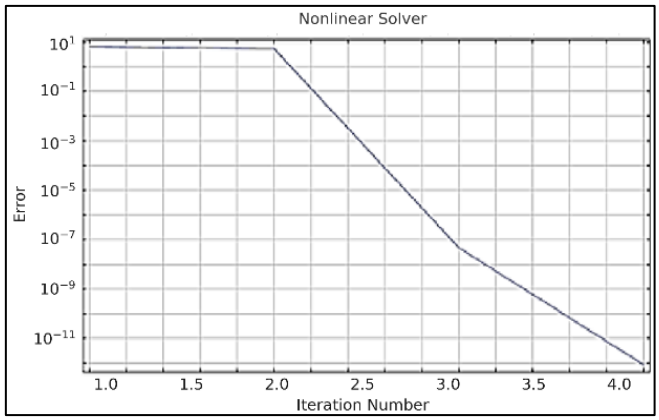

Figure 5. Error versus iteration number in the nonlinear solver showing exponential convergence within 4 iterations during the time-dependent simulation of the capacitive deionization model

The simulation parameters were set as follows: a relative tolerance of 1×10^{-4}, absolute tolerances of 1×10^{-6} V for potential and 1×10^{-5} mol/m³ for concentration, and an initial time step of 0.1 s (with a maximum step from 10 to100 s, and a minimum step of 1×10^{-5} s). As shown in Figure 5, simulations typically converged within four iterations, confirming numerical stability.

3. CAPACITIVE DEIONIZATION CELL MODELS

This study developed and simulated multiple CDI cell configurations using COMSOL Multiphysics 6.3 to evaluate desalination performance under membrane-free, stagnant water conditions using conductive concrete electrodes. The models incorporate realistic electrochemical properties and time-dependent ion transport mechanisms.

The electrochemical model integrates the following physics interfaces, as illustrated in Figure 6.

- Tertiary Current Distribution (TCD) – Nernst-Planck: Governs ion migration, diffusion, and electric field-driven convection across the full domain.
- Domain Ordinary Differential Equations (ODEs) and Differential-Algebraic Equations (DAEs) – Micropore Electrolyte Potential: Simulates potential gradients in the micropores using the modified Donnan approach.
- Domain ODEs – Attractive Potential: Captures non-electrostatic ion-pore surface interactions critical to electrosorption efficiency.

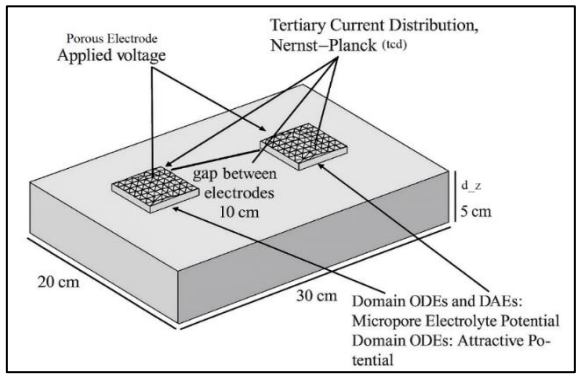

Figure 6. Schematic illustration of the electrochemical simulation model and the applied physics interfaces

3.1 Model for applied voltage variation

This model investigates the influence of applied voltage (5–25 V) on ion removal efficiency. Simulations were performed at an initial NaCl concentration of 7.2 mM (420 ppm), a temperature of 20°C, and an electrode spacing of 10 cm. The electric field generated by the applied DC voltage drives Na^+ and Cl^- ions toward the cathode and anode, respectively.

Performance metrics include temporal reduction in salt concentration, enabling assessment of how increasing electric field strength enhances electroadsorption kinetics and desalination capacity.

3.2 Model for electrode spacing variation

The specific energy consumption (SEC) was evaluated by integrating the instantaneous electrical power over the adsorption cycle and normalizing it by the treated water volume. The expression is given as:

$$\mathrm{SEC}\left(\mathrm{KWh/m^3}\right)=\frac{1}{3600}\times\frac{1}{wV}\int V(t)I(t)dt \tag{13}$$

where, $V(t)$ is the cell voltage, $I(t)$ is the current, t is the operation time, and V_w is the treated water volume [25-27].

3.3 Model for initial NaCl concentration variation

To examine the geometric influence, electrode gaps of 5, 7.5, 10, and 12.5 cm were simulated under constant voltage (15 V) and temperature (20°C), with 420 ppm NaCl. The model captures ion migration dynamics and electric potential distribution.

Figure 7 visualizes the electric field strength and potential contours for each spacing case. Closer spacing results in stronger fields, promoting faster ion migration, while wider gaps reduce electric field intensity and desalination performance.

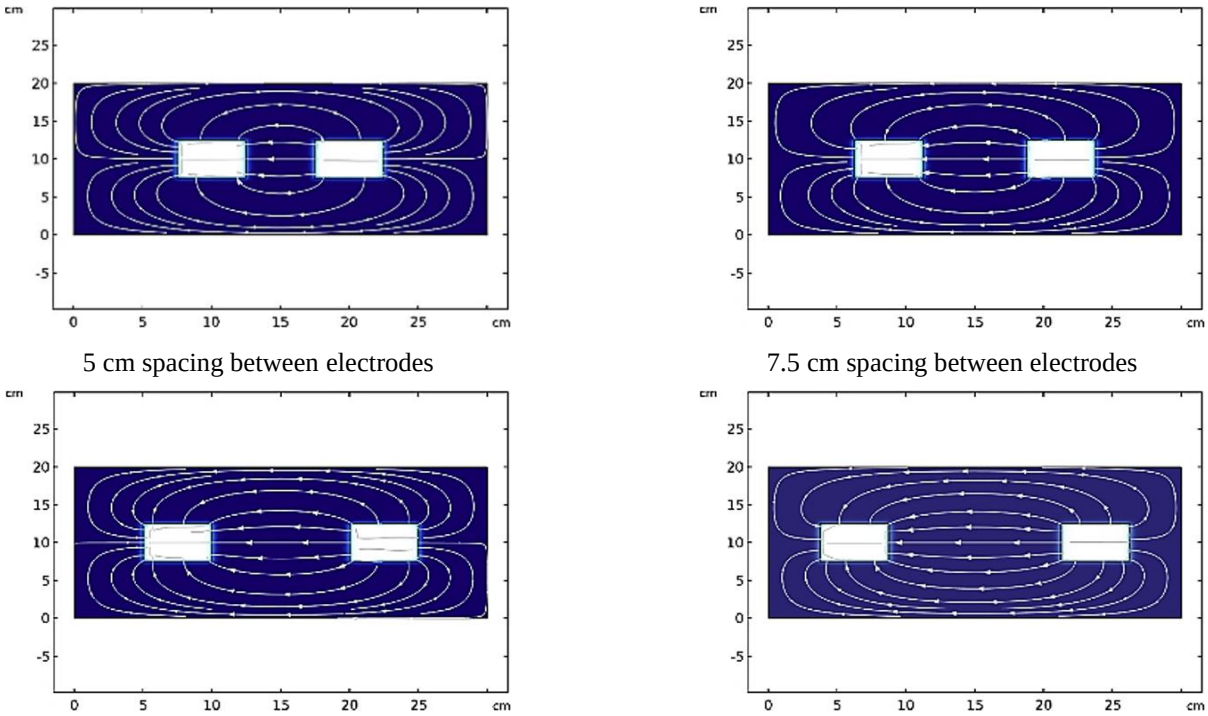

5 cm spacing between electrodes

7.5 cm spacing between electrodes

10 cm spacing between electrodes

12.5 cm spacing between electrodes

Figure 7. Spacing between electrodes and diffusion field intensity

Table 1. NaCl concentrations used in the theoretical study

Case	Concentration (ppm)	Equivalent (mM)	Description
Low salinity	250	4.28	Safe drinking water (WHO limit)
Moderate salinity	500	8.55	Upper limit of potable water
Brackish water	1000	17.1	Saline water suitable for limited irrigation
High brackish water	2000	34.2	Moderately saline (irrigation threshold)
Basra case	8000	136.9	Reported salinity in Basra (Iraq)

Note: ppm = parts per million; mM = millimolar (millimoles per liter).

3.4 Model for initial NaCl concentration variation

To investigate the influence of feedwater salinity on CDI performance, a numerical model was developed using COMSOL Multiphysics 6.3. The study assessed the system's ion removal efficiency under a range of initial NaCl concentrations representing typical and extreme water quality scenarios, from mildly brackish water to highly saline conditions.

Simulations were conducted under fixed operating parameters: an applied voltage of 15 V, a temperature of 25°C, and an electrode spacing of 7.5 cm. The selected concentrations encompass internationally accepted limits for potable water as well as real-world values reported in southern Iraq (Basra), where saltwater intrusion from the Shatt Al-Arab River has led to salinity levels exceeding 10,000 ppm,

especially during dry seasons [28]. Table 1 presents the modeled NaCl concentrations in both ppm and millimolar (mM), using the molar mass of NaCl (58.44 g/mol) for conversion. While actual salinity peaks in Basra may surpass 10,000 ppm, the simulation focused on a high-salinity benchmark of 8,000 ppm to ensure computational stability while capturing the extent of degradation in water quality. This range provides a robust basis for analyzing the relationship between inlet concentration and CDI desalination efficiency.

3.5 Study of production rate in large-scale capacitive deionization tanks

- Both tanks were modeled as cuboidal domains filled with stagnant NaCl solution (initial concentration ~8,000 ppm). Porous conductive concrete electrodes were placed on two opposite vertical walls, while the remaining faces were defined as insulating boundaries.
- **1000 L Tank (1 m³):** Modeled with dimensions of 1 m × 1 m × 1 m and a 1 m electrode spacing. A voltage range of 15–60 V was applied to evaluate performance over 24 hours (Figure 8).

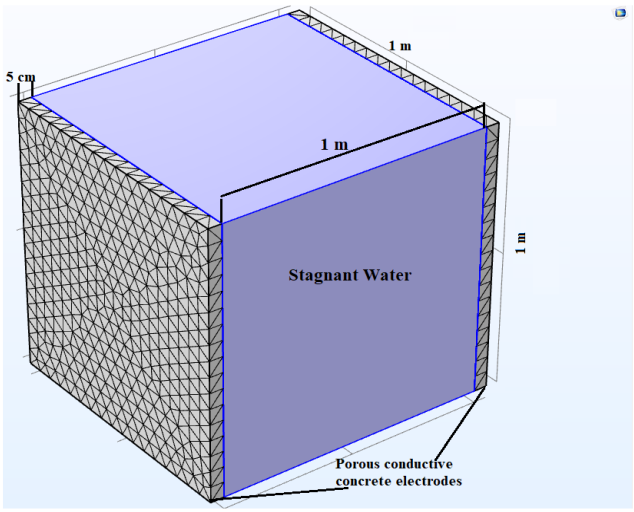

Figure 8. Capacitive deionization cell model for a 1000-liter (1 m³) tank with porous conductive concrete electrodes

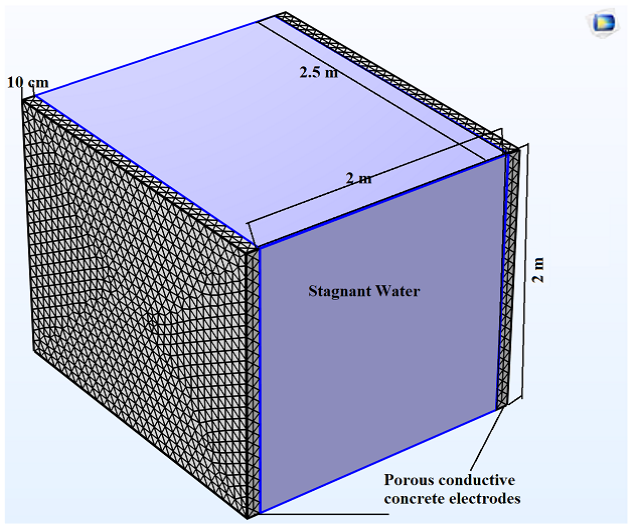

Figure 9. COMSOL model of a 10,000-liter (10 m³) capacitive deionization cell with porous conductive concrete electrodes

- **10000 L Tank (10 m³):** Simulated with dimensions of 2 m × 2 m × 2.5 m and a 2 m electrode spacing. Applied voltages ranged from 15 to 80 V to maintain sufficient ion transport while avoiding water electrolysis (Figure 9).

These simulations enabled a comparative analysis of ion removal kinetics and volumetric production capacity at different voltages. Voltage ranges were selected to optimize performance, ensuring efficient ion migration while minimizing energy consumption and potential electrode degradation.

4. RESULTS AND DISCUSSION

This section presents the numerical simulation results of electrochemical desalination using a CDI cell with conductive concrete electrodes. Simulations were performed in COMSOL Multiphysics 6.3, evaluating the effects of key operational parameters including applied voltage, electrode spacing, water temperature, and initial NaCl concentration.

The results provide insight into the spatial and temporal behavior of Na^+ and Cl^- ions in a stagnant saline environment. Ion accumulation near the respective electrodes and electric field development across the cell were clearly observed.

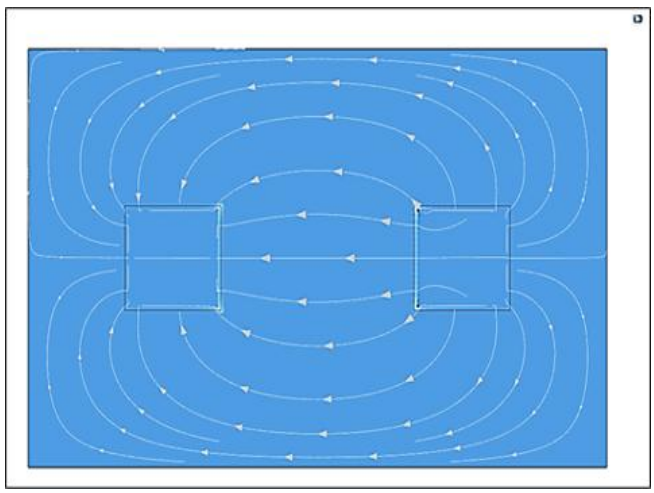

Figure 10. Simulated surface concentration of Na^+ ions, showing migration toward the cathode

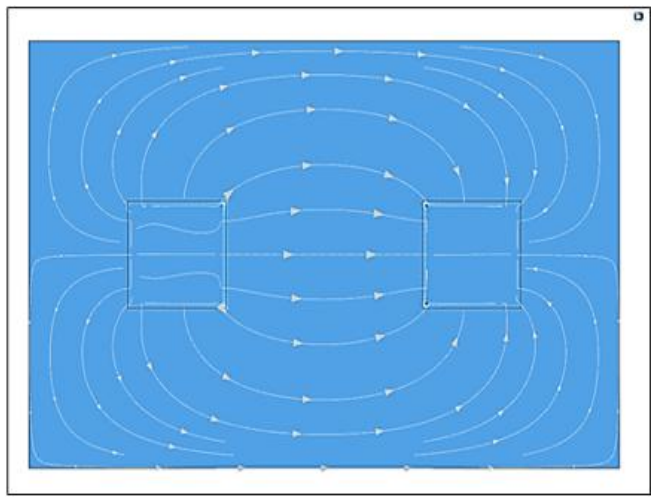

Figure 11. Simulated surface concentration of Cl^- ions, showing directional migration toward the anode

Figures 10 and 11 illustrate the surface concentrations of Na^+ and Cl^- ions under an applied DC voltage. Na^+ ions migrate toward the cathode (left), while Cl^- ions move toward the anode (right). The superimposed streamlines confirm directional ion migration and electroadsorption driven by the electric field. Edge effects and curvature near electrode corners further validate the model's accuracy in capturing transport dynamics.

This section presents the numerical simulation results of the electrochemical desalination process using a CDI cell equipped with conductive concrete electrodes. The simulations were conducted using COMSOL Multiphysics 6.3, focusing on the various operational parameters such as the applied voltage, inter-electrode spacing, water temperature, and ionic concentration.

These results offer insight into the spatiotemporal transport of Na^+ and Cl^- ions within the stagnant saline water domain, their accumulation near the respective electrodes, and the development of electric fields and attractive electrostatic potentials inside the CDI cell [29, 30].

4.1 Study the capacitive deionization cell at different voltages applied

Figure 12 displays the time-dependent NaCl concentration at various applied voltages (5–25 V). A higher applied voltage correlates with faster and deeper ion removal. Starting from 420 ppm, the concentration dropped to 228 ppm at 5 V, 189 ppm at 10 V, 127 ppm at 15 V, 96 ppm at 20 V, and 91 ppm at 25 V after 3600 seconds. These findings affirm that a stronger electric field accelerates ion migration and enhances electrosorption efficiency, consistent with the EDL theory [31-35].

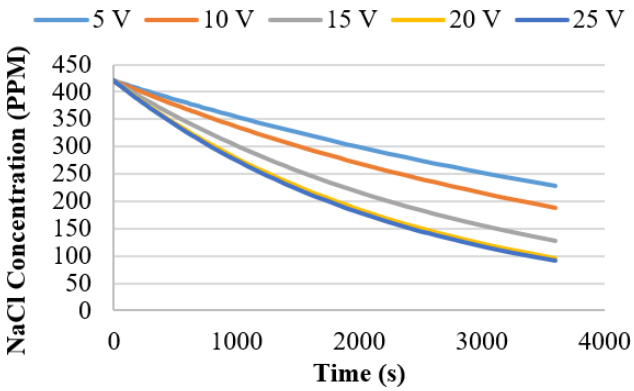

Figure 12. Variation of NaCl concentration over time at different applied voltages (5–25 V)

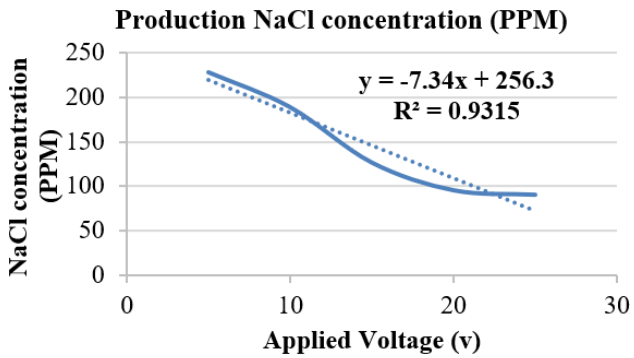

Figure 13. Effect of applied voltage on residual NaCl concentration after the CDI process

Figure 13 shows the linear relationship between applied voltage and final NaCl concentration. The regression model (R^2 = 0.9315) confirms that each 1 V increase results in approximately 7.34 ppm reduction in salinity, validating the voltage-dependence of CDI efficiency.

4.2 Specific energy consumption

The SEC was calculated based on the experimental data for NaCl removal at different applied voltages (5–25 V) using a 2 L batch CDI cell. The SEC was calculated from the time-integrated electrical energy normalized by the treated water volume according to Eq. (13) as shown in Table 2.

Table 2. Estimated specific energy consumption values compared with literature ranges

Applied Voltage (V)	Final Concentration (ppm)	Amount of Salt Removed (ppm)	Specific Energy Consumption (SEC) (kWh/m³)
5	200	220	0.59
10	185	235	1.27
15	135	285	2.31
20	100	320	3.45
25	90	330	4.45

In this study, the treated volume was 2 L. The current was estimated from the salt adsorption using Faraday's law, assuming a charge efficiency of 0.85 and monovalent NaCl ions.

The results show that SEC obtained SEC values (0.59–4.45 kWh/m³) that fall within or near the reported ranges for CDI (0.5–3 kWh/m³) [26, 27]. These comparisons confirm that Ag/rGO-enhanced conductive concrete electrodes can achieve competitive energy performance.

4.3 Study the effect of electrode spacing

Electric field behavior varies with electrode spacing. At 5 cm spacing, the field is intense and confined, enabling rapid and efficient ion transport, but with reduced coverage near sidewalls. Wider spacing (10–12.5 cm) leads to weaker, more dispersed fields, decreasing overall efficiency.

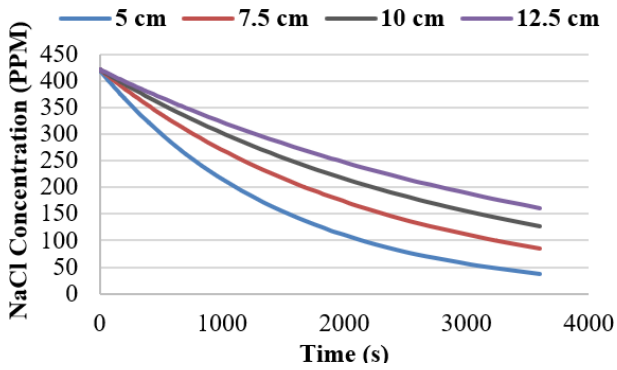

Figure 14. Effect of electrode spacing on NaCl concentration reduction over time at constant applied voltage

Figure 14 presents the influence of different electrode spacings, specifically 5, 7.5, 10, and 12.5 cm, on the reduction of NaCl concentration over a (3600 s) period under 15 V voltage conditions. Moderate spacing (7.5 cm) achieved a balance between field intensity and domain coverage. The

results indicate that shortening the electrode spacing significantly improves the electrosorption performance and electric field intensity, which leads to improved desalination efficiency [36].

This behavior is consistent with previous findings that show how field line concentration improves charge transport and electroadsorption efficiency at narrower electrode gaps [29-30]. This reduces the electrostatic driving force, especially in the middle region, and may lead to slower ion transport and diminished desalination performance [35]. However, this narrow spacing also increases the gap between the electrodes and the sidewalls of the cell, reducing the field's reach to the outer regions. As a result, while ion removal in the central path improves, peripheral areas may retain higher salt concentrations [37].

These findings demonstrate that reduced spacing enhances the electric field strength and electrosorption performance, but extremely narrow gaps may limit lateral coverage. Optimal performance is achieved between 5 and 7.5 cm spacing.

Overall, the analysis confirms that minimizing electrode spacing strengthens the electric field and accelerates ion transport, resulting in more efficient removal of salt from the solution.

4.4 Effect of initial NaCl concentration on capacitive deionization performance

To evaluate the impact of feedwater salinity on CDI performance, a range of initial NaCl concentrations was simulated using COMSOL Multiphysics under fixed operating conditions: 15 V applied voltage, 25°C temperature, and 7.5 cm electrode spacing. The selected concentrations represent realistic scenarios ranging from brackish water (250–500 ppm) to highly saline conditions (8,000 ppm), such as those reported in Basra, Iraq, due to saltwater intrusion. At low salinity (250 and 500 ppm), the CDI cell performs efficiently, achieving final concentrations below 100 ppm after 1 hour, consistent with earlier observations that efficient charge transfer and minimized electrode saturation occur at low ionic concentrations [38].

Simulation results reveal that NaCl concentration decreases over time in all cases, confirming active electroadsorption. However, the efficiency of ion removal is strongly influenced by the initial salinity:

- **Low salinity (250–500 ppm):** Rapid and efficient desalination is observed, with final concentrations dropping below 100 ppm after 1 hour. This agrees with Shocron and Suss [16], who reported enhanced charge transfer and minimized electrode saturation at low ionic strengths.
- **Moderate salinity (1,000–2,000 ppm):** Ion removal continues but at a slower rate. As Uralcan et al. [17] noted, higher ionic strength leads to condensed ionic adlayers and less uniform charge distribution within the electric double layer, reducing adsorption efficiency.
- **High salinity (8,000 ppm):** The CDI cell exhibits the slowest performance, with residual concentrations exceeding 3,000 ppm. This is consistent with Rommerskirchen et al. [18], who found that compressed electric double layers at high salinity hinder electrostatic attraction and ion transport.

Figure 15 presents the aggregated system behavior under these varying salinity levels. These findings underscore that the initial NaCl concentration is a critical factor governing CDI efficiency. Lower salinity enhances electroadsorption and charge efficiency, while higher salinity introduces limitations in electric field-driven separation and double-layer capacity.

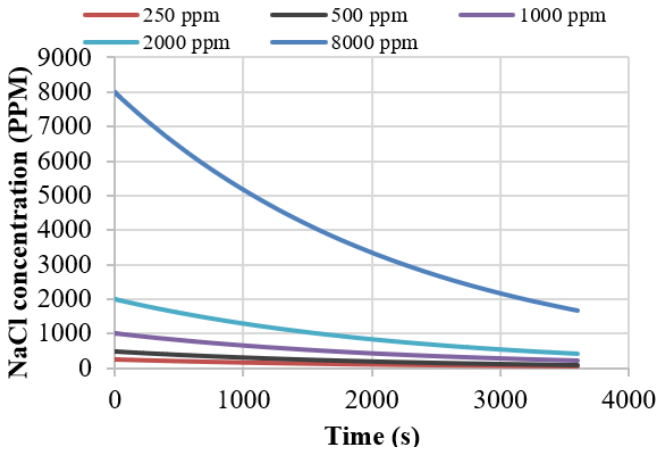

Figure 15. ppm after 1 hour at various initial concentrations

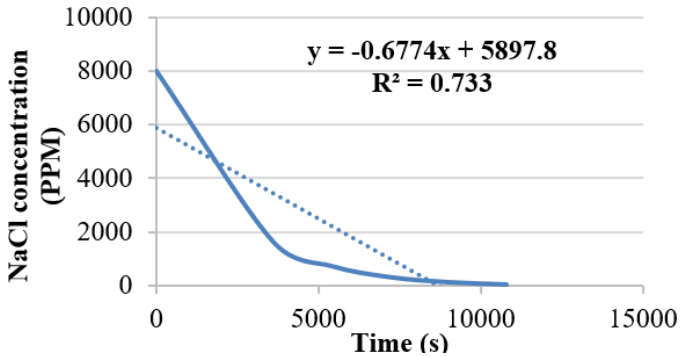

Figure 16. ppm as a function of time showing progressive electroadsorption efficiency over 3 hours of capacitive deionization operation at 15 V applied voltage, 7.5 cm spacing between electrodes, and at 25°C

4.5 Effect of extended operation time on NaCl concentration reduction

Simulation results indicate a clear time-dependent improvement in CDI performance: as operating time increases from 1 to 3 hours, the NaCl concentration in the treated water steadily decreases Figure 16. This reflects progressive electroadsorption driven by continued ion transport toward the electrodes. At 1 hour, the concentration decreases from 8,000 ppm to 1,664 ppm. By 3 hours, it drops significantly to 72 ppm, well below the WHO-recommended limit for drinking water (< 500 ppm). This prolonged exposure enhances electric double layer formation and charge transfer efficiency, particularly critical for high-salinity scenarios such as those found in Basra, Iraq, where salinity often exceeds 8,000–10,000 ppm.

These findings align with previous studies: Shocron and Suss [16] demonstrated that extended charging enhances ion uptake, while Rommerskirchen et al. [18] emphasized the role of prolonged operation in overcoming diffusion limitations and electrode saturation.

The data follow a linear trend described by the regression equation:

$$y = -0.6774x + 5897.8$$

where, y is ppm and x is time (s). The negative slope confirms the downward trend, though the moderate R^2 value (0.733) suggests diminishing returns beyond 1 hour due to electrode saturation and equilibrium effects.

Table 3. Time-dependent ppm in the 1000-liter capacitive deionization tank at various voltages (15–50 V) over 24 hours

Time (h)	15 V	20 V	25 V	30 V	35 V	40 V	45 V	50 V
0	8000	8000	8000	8000	8000	8000	8000	8000
1	7019	6719	6433	6158	5896	5644	5403	5173
2	6158	5644	5173	4741	4345	3982	3649	3344
3	5403	4741	4159	3649	3202	2809	2465	2162
4	4741	3982	3344	2809	2359	1982	1664	1398
5	4159	3344	2689	2162	1739	1398	1124	904
6	3649	2809	2162	1664	1281	986	759	584
8	2809	1982	1398	986	696	491	346	244
10	2162	1398	904	584	378	244	158	102
12	1664	986	584	346	205	121	72	42
14	1281	696	378	205	111	60	32	17
16	986	491	244	121	60	30	15	7
18	759	346	158	72	32	15	6	3
20	584	244	102	42	17	7	3	1
22	450	172	66	25	9	3	1	0.5
24	346	121	42	15	5	1	0.6	0.2

Table 4. Time-dependent ppm in the 10000-liter capacitive deionization tank at various voltages (15–80 V) over 24 hours

Time (h)	15 V	20 V	30 V	40 V	50 V	60 V	70 V	80 V
0	8000	8000	8000	8000	8000	8000	8000	8000
1	7543	7396	7111	6838	6575	6322	6078	5844
2	7111	6838	6322	5844	5403	4995	4618	4270
4	6322	5844	4995	4270	3649	3119	2666	2279
6	5619	4995	3947	3119	2465	1947	1539	1216
8	4995	4270	3119	2279	1664	1216	888	649
10	4440	3649	2465	1664	1124	759	513	346
12	3947	3119	1947	1216	759	474	296	184
14	3509	2666	1539	888	513	296	170	98
16	3119	2279	1216	649	346	184	98	52
18	2773	1947	961	474	234	115	56	28
20	2465	1664	759	346	158	72	32	15
22	2191	1423	600	253	106	45	18	8
24	1947	1216	474	184	72	28	10	4

4.6 Production rate in large-scale capacitive deionization tanks

4.6.1 The simulation results for the 1000-liter CDI tank

A static 1,000-liter CDI tank was simulated to evaluate the effect of applied voltage (15–50 V) on NaCl removal over a 24-hour batch cycle. The system began with an initial salinity of 8,000 ppm. Results in Table 3 show that:

- Low voltages (15–25 V): Desalination is slow, with outlet concentrations remaining above 2,000 ppm after 10 hours and only reaching potable levels (< 500 ppm) after 20 hours.
- High voltages (30–50 V): Salt removal is substantially faster. At 50 V, the concentration drops below 500 ppm in under 10 hours and reaches < 100 ppm by the end of the cycle.

The optimal operating window is 35–45 V, balancing effective desalination, energy efficiency, and system longevity. Within this range, salinity drops to < 500 ppm in approximately 10–12 hours. Accounting for tank drainage, electrode regeneration, and refilling (2–3 hours), the system supports two full batch cycles per day, enabling production of about 2000 liters/day of potable water.

4.6.2 The simulation results for the 10000-liter capacitive deionization tank

The 10000-liter CDI tank was simulated to assess desalination performance under voltages ranging from 15 to 80 V. According to Table 4.

- Lower voltages (15–30 V): Desalination remains inefficient, with outlet salinity exceeding 3000 ppm even after 12 hours of operation.
- Higher voltages (60–80 V): Salt removal improves significantly. At 80 V, the concentration decreases to < 500 ppm within 12–14 hours and reaches < 100 ppm by the end of the cycle.

The optimal voltage range of 60–80 V ensures rapid desalination with manageable energy use and electrode stress. With additional time (2–3 hours) for flushing and refilling, each batch cycle lasts 14–17 hours, enabling up to 1.5 cycles/day and about 15000 liters/day of treated water under continuous operation.

4.7 Numerical and experimental results validation

To check the accuracy of the simulation model, a laboratory experiment was carried out using a 2-liter CDI cell with the same dimensions as the one used in the simulation. The NaCl concentration was measured over time under applied voltages of 5 V, 10 V, 15 V, 20 V, and 25 V. As illustrated in Figure 17, both the experimental and simulation results show a steady decrease in NaCl concentration over time. Higher voltages resulted in more efficient ion removal, confirming that stronger electric fields enhance the electroadsorption capacity. At 5 V, the simulation slightly overpredicts the removal rate compared to the experimental results, likely because the model assumes ideal conditions and does not account for factors like salt buildup on the electrodes. At voltages of 15 V and above, the simulation results closely match the experimental data, indicating that the model successfully captures the main

processes, including EDL formation, ion migration, and adsorption behavior under higher electric fields.

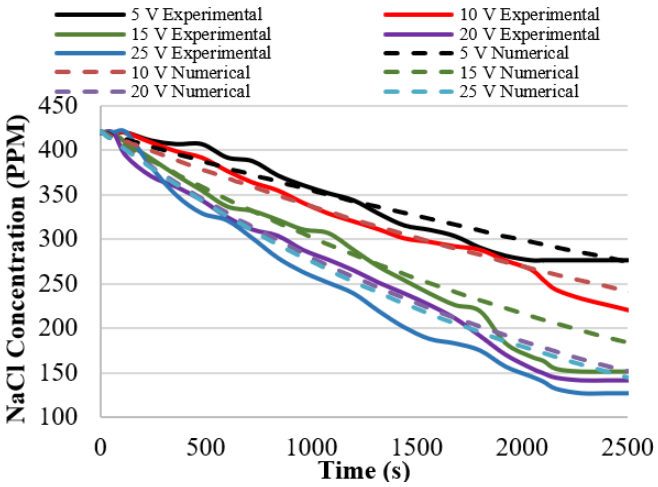

Figure 17. Comparison of experimental and numerical NaCl concentration vs. time at different applied voltages

Table 5. The validation of numerical and experimental salt removal efficiency at different applied voltages

Applied Voltage (V)	Experimental Efficiency (%)	Numerical Efficiency (%)
5	34.04	45.7
10	49.76	55
15	64.05	69.7
20	66.42	77.1
25	69.7	78.4

Table 5 illustrates the comparison between experimental and numerical salt removal efficiencies at various applied voltages ranging from 5 V to 25 V. The salt removal efficiency was computed using the equation:

$$\text{Salt removal efficiency (\%)} = \frac{\text{Initial concentration} - \text{Final concentration}}{\text{Initial concentration}} \times 100\%$$

5. CONCLUSION

In this study, a model was developed to simulate CDI by using conductive concrete electrodes enhanced with Ag/rGO nanocomposites. The numerical model was evaluated using applied voltage, electrode spacing, water salinity, and operating time. The results proved that high voltage improved ion removal, with the highest reduction in NaCl concentration achieved at 25 V. Reducing the electrode spacing enhanced the electric field intensity, and lower salinity levels with faster desalination rates. Furthermore, extending the operation time allowed for effective treatment of high-salinity water. The simulations confirmed that under optimized conditions, a 10 m^3 system could produce up to 15,000 L/day of potable water, which is suitable for regions like Basra, Iraq. While the electrodes showed promising performance, the study did not cover long-term durability, fouling, or chemical interactions, which should be addressed in future research to ensure environmental safety and sustainability. The SEC values (0.59–4.45 kWh/m^3) indicate that the developed Ag/rGO-based conductive concrete electrodes demonstrate competitive energy efficiency, further supporting their potential for practical desalination applications. Nevertheless, the present study has several limitations. The simulations assume ideal conditions, neglecting parasitic reactions, thermal effects, and aging of the composite electrodes.

REFERENCES

[1] Torkamanzadeh, M., Kök, C., Burger, P.R., Ren, P., Zhang, Y., Lee, J., Kim, C., Presser, V. (2023). Best practice for electrochemical water desalination data generation and analysis. Cell Reports Physical Science, 4(11). https://doi.org/10.1016/j.xcrp.2023.101661

[2] Alkhadra, M.A., Gao, T., Conforti, K.M., Tian, H., Bazant, M.Z. (2020). Small-scale desalination of seawater by shock electrodialysis. Desalination, 476: 114219. https://doi.org/10.1016/j.desal.2019.114219

[3] Gamaethiralalage, J.G., Singh, K., Sahin, S., Yoon, J., Elimelech, M., Suss, M.E., Liang, P., Biesheuvel, P.M., Zornitta, R.L., De Smet, L.C.P.M. (2021). Recent advances in ion selectivity with capacitive deionization. Energy and Environmental Science, 14(3): 1095-1120. https://doi.org/10.1039/d0ee03145c

[4] Kumar, S., Aldaqqa, N.M., Alhseinat, E., Shetty, D. (2023). Electrode materials for desalination of water via capacitive deionization. Angewandte Chemie, 135(35): e202302180. https://doi.org/10.1002/ange.202302180

[5] Wang, H., Yan, T., Shen, J., Zhang, J., Shi, L., Zhang, D. (2020). Efficient removal of metal ions by capacitive deionization with straw waste derived graphitic porous carbon nanosheets. Environmental Science: Nano, 7(1): 317-326. https://doi.org/10.1039/c9en01233h

[6] Mahmud, N., Alvarez, D.V.F., Ibrahim, M.H., El-Naas, M.H., Esposito, D.V. (2022). Magnesium recovery from desalination reject brine as pretreatment for membraneless electrolysis. Desalination, 525: 115489. https://doi.org/10.1016/j.desal.2021.115489

[7] Porada, S., Zhao, R., van der Wal, A., Presser, V., Biesheuvel, P.M. (2013). Review on the science and technology of water desalination by capacitive deionization. Progress in Materials Science, 58(8): 1388-1442. https://doi.org/10.1016/j.pmatsci.2013.03.005

[8] Farmer, J.C., Fix, D.V., Mack, G.V., Pekala, R.W., Poco, J.F. (1996). Capacitive deionization of NaCl and $NaNO_3$ solutions with carbon aerogel electrodes. Journal of the Electrochemical Society, 143(1): 159. https://doi.org/10.1149/1.1836402

[9] Biesheuvel, P.M. (2009). Thermodynamic cycle analysis for capacitive deionization. Journal of Colloid and Interface Science, 332(1): 258-264. https://doi.org/10.1016/j.jcis.2008.12.018

[10] Biesheuvel, P.M., Bazant, M.Z. (2010). Nonlinear dynamics of capacitive charging and desalination by porous electrodes. Physical Review E-Statistical, Nonlinear, and Soft Matter Physics, 81(3): 031502. https://doi.org/10.1103/PhysRevE.81.031502

[11] Jiang, Y., Li, K., Alhassan, S.I., Cao, Y., et al. (2022). Spinel $LiMn_2O_4$ as a capacitive deionization electrode material with high desalination capacity: Experiment and simulation. International Journal of Environmental Research and Public Health, 20(1): 517. https://doi.org/10.3390/ijerph20010517

[12] Nordstrand, J., Zuili, L., Toledo-Carrillo, E.A., Dutta, J.

(2022). Predicting capacitive deionization processes using an electrolytic-capacitor (ELC) model: 2D dynamics, leakages, and multi-ion solutions. Desalination, 525: 115493. https://doi.org/10.1016/j.desal.2021.115493
[13] Nordstrand, J., Zuili, L., Dutta, J. (2023). Fully 3D modeling of electrochemical deionization. ACS Omega, 8(2): 2607-2617. https://doi.org/10.1021/acsomega.2c07133
[14] Seyedhassantehrani, N., Palko, J.W. (2023). Outflow geometry for electrochemical desalination cells. Electrochimica Acta, 449: 142180. https://doi.org/10.1016/j.electacta.2023.142180
[15] Haverkort, J.W., Sanderse, B., Padding, J.T., Blake, J.W. (2024). An analytical flow-by capacitive deionization model. Desalination, 582: 117408. https://doi.org/10.1016/j.desal.2024.117408
[16] Shocron, A.N., Suss, M.E. (2017). The effect of surface transport on water desalination by porous electrodes undergoing capacitive charging. Journal of Physics: Condensed Matter, 29(8): 084003. https://doi.org/10.1088/1361-648X/29/8/084003
[17] Uralcan, B., Aksay, I.A., Debenedetti, P.G., Limmer, D.T. (2016). Concentration fluctuations and capacitive response in dense ionic solutions. The Journal of Physical Chemistry Letters, 7(13): 2333-2338. https://doi.org/10.1021/acs.jpclett.6b00859
[18] Rommerskirchen, A., Linnartz, C.J., Egidi, F., Kendir, S., Wessling, M. (2020). Flow-electrode capacitive deionization enables continuous and energy-efficient brine concentration. Desalination, 490: 114453. https://doi.org/10.1016/j.desal.2020.114453
[19] Yehia, S. (2004). Implementation of conductive concrete overlay for bridge deck deicing at Roca, Nebraska. Civil Engineering Faculty Proceedings & Presentations, 6: 363-378. https://digitalcommons.unomaha.edu/civilengfacproc.
[20] Chang, C., Ho, M., Song, G., Mo, Y.L., Li, H. (2009). A feasibility study of self-heating concrete utilizing carbon nanofiber heatingelements. Smart Materials and Structures, 18(12): 127001. https://doi.org/10.1088/0964-1726/18/12/127001
[21] Ahmed, S., Hussain, A., Hussain, Z., Pu, Z., Ostrowski, K.A., Walczak, R. (2021). Effect of carbon black and hybrid steel-polypropylene fiber on the mechanical and self-sensing characteristics of concrete considering different coarse aggregates' sizes. Materials, 14(23): 7455. https://doi.org/10.3390/ma14237455
[22] Downey, A., D'Alessandro, A., Baquera, M., García-Macías, E., et al. (2017). Damage detection, localization and quantification in conductive smart concrete structures using a resistor mesh model. Engineering Structures, 148: 924-935. https://doi.org/10.1016/j.engstruct.2017.07.022
[23] Khalid, T., Albasha, L., Qaddoumi, N., Yehia, S. (2017). Feasibility study of using electrically conductive concrete for electromagnetic shielding applications as a substitute for carbon-laced polyurethane absorbers in anechoic chambers. IEEE Transactions on Antennas and Propagation, 65(5): 2428-2435. https://doi.org/10.1109/TAP.2017.2670538
[24] Stratfull, R.F. (1974). Experimental Cathodic Protection of a Bridge Deck (No. 500).
[25] Tarus, B.K., Ullah, Z., Jande, Y.A., Njau, K.N., Byun, J., Son, M. (2024). Desalination performance in versatile capacitive/battery deionization configurations using a cation intercalating electrode. Desalination, 586: 117857. https://doi.org/10.1016/j.desal.2024.117857
[26] Hawks, S.A., Ramachandran, A., Porada, S., Campbell, P.G., et al. (2019). Performance metrics for the objective assessment of capacitive deionization systems. Water Research, 152: 126-137. https://doi.org/10.1016/j.watres.2018.10.074
[27] Song, J., Ma, J., Zhang, C., He, C., Waite, T.D. (2019). Implication of non-electrostatic contribution to deionization in flow-electrode CDI: Case study of nitrate removal from contaminated source waters. Frontiers in Chemistry, 7: 146. https://doi.org/10.3389/fchem.2019.00146
[28] UNICEF. (2019). Multi-tiered approaches to solving the water crisis in Basra, Iraq. UNICEF Report. https://www.unicef.org/media/91401/file/Multi-Tiered-Approaches-to-Solving-the-Water-Crisis-in-Basra-Iraq.pdf.
[29] Hemmatifar, A., Stadermann, M., Santiago, J.G. (2015). Two-dimensional porous electrode model for capacitive deionization. The Journal of Physical Chemistry C, 119(44): 24681-24694. https://doi.org/10.1021/acs.jpcc.5b05847
[30] Suss, M.E., Porada, S., Sun, X., Biesheuvel, P.M., Yoon, J., Presser, V. (2015). Water desalination via capacitive deionization: What is it and what can we expect from it? Energy & Environmental Science, 8(8): 2296-2319. https://doi.org/10.1039/C5EE00519A
[31] Lado, J.J., Wouters, J.J., Tejedor-Tejedor, M.I., Anderson, M.A., García-Calvo, E. (2013). Asymmetric capacitive deionization utilizing low surface area carbon electrodes coated with nanoporous thin-films of Al_2O_3 and SiO_2. Journal of The Electrochemical Society, 160(8): E71. https://doi.org/10.1149/2.094308jes
[32] Ahmed, M.A., Tewari, S. (2018). Capacitive deionization: Processes, materials and state of the technology. Journal of Electroanalytical Chemistry, 813: 178-192. https://doi.org/10.1016/j.jelechem.2018.02.024
[33] Elisadiki, J., Kibona, T.E., Machunda, R.L., Saleem, M.W., Kim, W.S., Jande, Y.A. (2020). Biomass-based carbon electrode materials for capacitive deionization: A review. Biomass Conversion and Biorefinery, 10(4): 1327-1356. https://doi.org/10.1007/s13399-019-00463-9
[34] Chen, R., Sheehan, T., Ng, J.L., Brucks, M., Su, X. (2020). Capacitive deionization and electrosorption for heavy metal removal. Environmental Science: Water Research & Technology, 6(2): 258-282. https://doi.org/10.1039/C9EW00945K
[35] Bao, S., Xin, C., Zhang, Y., Chen, B., Ding, W., Luo, Y. (2023). Application of capacitive deionization in water treatment and energy recovery: A review. Energies, 16(3): 1136. https://doi.org/10.3390/en16031136
[36] Thungsuai, K., Pimpha, N., Chaleawlert-umpon, S. (2022). Influence of carbon electrode thickness and spacing on capacitive deionization performance. Research Square Preprint. https://doi.org/10.21203/rs.3.rs-1909665/v1
[37] Długołecki, P., van der Wal, A. (2013). Energy recovery in membrane capacitive deionization. Environmental Science & Technology, 47(9): 4904-4910. https://doi.org/10.1021/es3053202
[38] Jiang, Y., Alhassan, S.I., Wei, D., Wang, H. (2020). A

review of battery materials as CDI electrodes for desalination. Water, 12(11): 3030. https://doi.org/10.3390/w12113030

NOMENCLATURE

Latin symbols

A	Electrode surface area, m²
C	Salt concentration, mg/L or mol/m³
C_o	Initial salt concentration, mg/L or mol/m³
C_t	Salt concentration at time t, mg/L or mol/m³
ΔC	Change in salt concentration, $C_o - C_t$, mg/L
CE	Charge efficiency, dimensionless
E	Energy consumption, kWh
I	Current, A
J	Current density, A/m²
L	Electrode spacing (gap length), m
n	Number of moles of salt removed, mol
Q	Electric charge, C
R	Universal gas constant, $J \cdot mol^{-1} \cdot K^{-1}$
SEC	Specific energy consumption, kWh/m³
t	Time, s
V	Applied voltage, V
V_w	Treated water volume, m³
η	Salt removal efficiency, % (dimensionless)

Greek symbols

Λ	Charge efficiency factor, dimensionless
μ	Dynamic viscosity of electrolyte, Pa·s
ρ	Density of solution, kg/m³
φ	Porosity of electrode, dimensionless

Subscripts

exp	Experimental
num	Numerical/simulation
in	Inlet
out	Outlet
e	Electrode
w	Water